Journal of Ship Research, Vol. 52, No. 4, December 2008, pp. 263–273

Unsteady Effects During Resistance Tests on a Ship Model in a Towing Tank

Lawrence J. Doctors,* **Alexander H. Day,**† and **David Clelland**†

*School of Mechanical and Manufacturing Engineering, The University of New South Wales, Sydney, Australia
†Department of Naval Architecture and Marine Engineering, The Universities of Glasgow and Strathclyde, Glasgow, Scotland

It is known that there are oscillations in the wave resistance during the constant-velocity phase of a towing-tank resistance test on a ship model. In this work, the unsteady thin-ship resistance theory has been applied to this case. The results have been compared with experiment data obtained using a towing carriage the velocity history of which can be programmed. It is demonstrated here that generally excellent correlation exists between the theory and the experiments. In particular, one can predict the influence of Froude number, rate of acceleration, and type of smoothing of the acceleration on the characteristics of the oscillations. These characteristics include the amplitude, rate of decay, frequency, and phasing of the oscillations in the curve of wave resistance versus time.

Keywords: hydrodynamics (general); model testing; resistance (general)

1. Introduction

1.1. Background

THE UNSTEADY RESISTANCE of a ship has been a little studied subject in comparison to the steady resistance. The latter topic has been intensively researched, in a mathematical sense, for well over a century, since the advent of the landmark paper of Michell (1898), who produced the first paper with a formula for predicting the wave resistance.

Although ships do spend the majority of their operational time sailing at a constant speed on a straight course, there are circumstances when unsteady effects can be important. These are during the acceleration and deceleration phases. In particular, even if one wished to conduct towing-tank tests on ship models, with the specific purpose of predicting the steady resistance of a prototype vessel in the equivalent condition (such as the same relative water depth) and the corresponding speed (the same Froude number), there remains the question of whether a steady-state condition has been reached during the experiment in the towing tank.

Sretensky (1936) is credited with extending the Michell theory, which is applicable to the case of a thin ship, to the situation of a vessel traveling along the center of a canal. It is an interesting aspect of the mathematical analysis that the addition of the constraints of the sidewalls of the canal yields an almost identical formula for the wave resistance. The only difference is that the integral over the wave numbers in the case of the laterally unconstrained case becomes a summation, in which the relevant discrete transverse wave numbers correspond to the wave components that can exist in the canal.

The Sretensky formulation was extended to the case of a finite water depth by Lunde (1951 and 1953). In this case, the formulas for the wave resistance still retain their general appearance, with two notable differences. First, the wave number for each wave component must satisfy a transcendental dispersion relationship. Second, the Michell wave functions (essentially integrals over the centerplane of the hull) take on a more elaborate character, involving hyperbolic functions of the water depth.

Lunde appears to be the first researcher who developed the analysis of the ship-wave problem to include the unsteady effects. In the general case of unsteady motion, one requires a triple integral for the wave resistance: a double integral over the longitudinal and transverse wave-number domain together with an integral over the time, from the start of the motion. On the other hand, the steady-state analysis leads to just a single integral or summa-

Manuscript received at SNAME headquarters, January 30, 2007; revised manuscript received December 5, 2007.

tion in the wave-number domain, because the dispersion relationship provides a unique connection between the longitudinal and the transverse wave numbers. Shebalov (1970) also contributed to the field of unsteady ship resistance.

There has also been an interest in applying the unsteady analysis to air-cushion vehicles, which can be represented by a pressure distribution on the free surface of the water. This work was initiated by Djachenko (1970). (This report is an English translation of the original Russian-language paper published in 1966.) This particular line of research was extended by Doctors and Sharma (1972, 1973). Their concern lay with the notion that the very high steady-state resistance peaks might be alleviated in the case of the more realistic unsteady motion. This work was characterized by including the results of numerical calculations, a feature missing from the abovementioned efforts of previous researchers.

Experiment confirmation of these predictions was published by Doctors (1975), for the simpler case of a two-dimensional pressure band undergoing a constant acceleration. It was demonstrated in that work that the linearized theory provides excellent predictions of the influence of acceleration on the resistance. This influence appears principally as a delay of the characteristic humps and hollows in the resistance curve to larger Froude numbers. This experiment work was later extended by Doctors (1993) to the practically more important case of a surface-effect ship model. It was shown that some of the very persistent unsteady effects, even after the model has been traveling at a constant speed for a long period of time, would correlate well with the theory.

The unsteady linearized theory referred to here can be applied equally well to the maneuvering of air-cushion vehicles. This has been done, but only in a purely theoretical manner, by Doctors (1972) and Haussling and Van Eseltine (1975 and 1978).

1.2. Current work

The current work has its origins in the unsteady theory developed by Lunde (1951, 1953). Our efforts were strongly motivated by the extraordinary paper by Wehausen (1964). Wehausen, using the theory of Lunde as a basis, developed asymptotic formulas for the unsteady wave resistance of a ship, applicable to the case when the vessel had reached a constant speed for a long period of time.

The Wehausen formulas, involving a long and intricate analysis, are remarkably simple in their final form. Essentially, the formula for the wave resistance for any particular constant-speed run depends on just one wave number (not a spectrum of wave numbers), corresponding to the group velocity of the transverse waves generated by the vessel. An additional factor in the formula is a decaying harmonic factor. The amplitude of the oscillations in the curve of wave resistance decays inversely with the time after the start of the motion, at least in the asymptotic sense.

The reader is also referred to the paper by Sibul, Webster, and Wehausen (1979), in which the starting phenomena were discussed on both a physical and mathematic basis. The work by Yeung (1975), being an extension of the research by Doctors (1972), was a great advance at that time, because the unsteady wave system itself (not just the overall wave resistance) was computed for the case of a maneuvering air-cushion vehicle. We should also add that the remarkable work of Wehausen (1964) was amplified to include the actual unsteady development of the wave pattern by Çalişal (1977) for the case of deep water and an infinitely wide towing tank.

The aim of the present investigation is to extend the work of Wehausen to the problem of a ship model test in a towing tank, in which both the width of the tank and the depth of the water are finite. In the work of Wehausen (1964), both of these parameters were considered to be infinite. Furthermore, it can be assumed that the asymptotic formulas of Wehausen may not be applicable immediately after the start of the constant-speed portion of the run in the towing tank.

This is a problem of considerable practical interest, since the unsteady effects both in resistance and in heave and pitch motions can clearly influence the quality of results obtained. In some cases, with certain vessels, the unsteady effects can be substantial and can decay relatively slowly, leaving oscillations still clearly visible in the data when the carriage brakes. Normal practice for the analysis of such oscillatory data is to take the average resistance over an integer number of cycles. This calculation requires some iteration, since the position of the "zero-crossings" defining the cycle depend on the a priori unknown average value; otherwise it is intrinsically straightforward. However, the assumption is implicitly made that the resistance oscillates symmetrically about the eventual steady-state value so that the decaying oscillatory variation is a zero-mean process. While Wehausen's formula suggests that this assumption is correct asymptotically in an unbounded fluid, it is of interest to confirm that the assumption is still correct in a real towing tank of finite dimensions a short time after a relatively rapid acceleration.

The interested reader is referred to the additional and more recent work on unsteady ship resistance, by Nakos and Sclavounos (1990), in which the wave pattern itself was the subject of interest. Time-domain calculations of the wave resistance were later implemented by Kara and Vassalos (2005). The subject of our planned tests was a Wigley (1934) model with standard proportions. The model has a length of 3.000 m, a waterline beam of 0.300 m, and a draft of 0.1875 m. A pictorial view and a body plan are shown in Fig. 1 (top).

The general form of the velocity history is depicted in Fig. 1 (bottom). The velocity history during the acceleration phase is divided into three subphases, followed by a phase of constant velocity, as follows:

$$U = \begin{cases} k_1 t^3 & \text{for} \quad 0 \le t \le t_A \\ k_2 + \dot{U}_{\max} t & \text{for} \quad t_A < t \le t_B \\ \overline{U} + k_3 (t - t_0)^3 & \text{for} \quad t_B < t \le t_0 \\ \overline{U} & \text{for} \quad t_0 < t \end{cases} . \tag{1}$$

The four unknowns in equation (1), namely k_1, k_2, k_3, and $\dot{U}_{\max}$, can be derived from the matching of the value and the slope of the function at the two internal break points. This general choice of carriage acceleration history permitted an exhaustive investigation into the effects of acceleration on the unsteady resistance of a ship model in a towing tank.

2. Theory

2.1. Governing equations

We consider the rectilinear motion of a ship model starting from rest and traveling along the centerline of a towing tank with a width w and filled with water to a depth d. A right-handed reference frame the origin of which is located at the undisturbed free

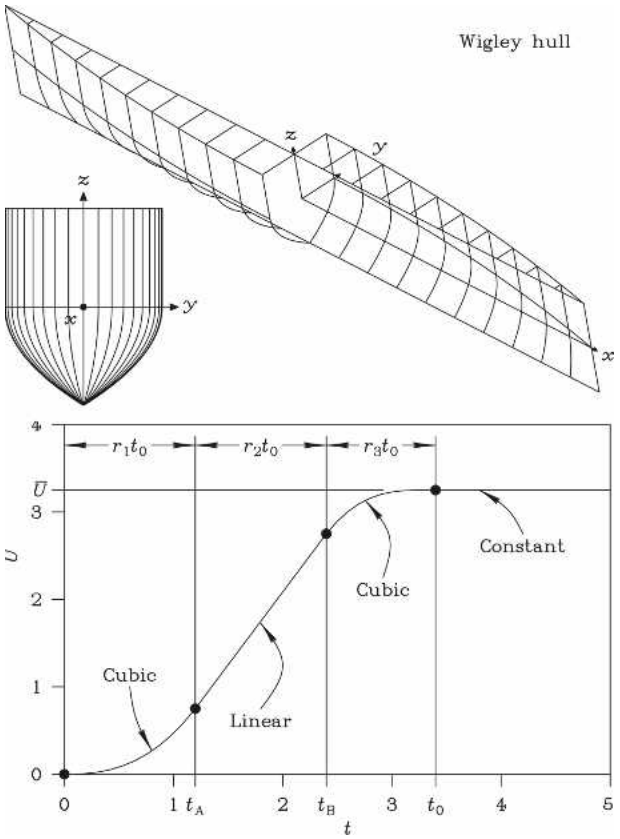

Fig. 1 Definition of the problem. (Top) Wigley model. (Bottom) Idealized velocity history

surface is used. We note that x is directed longitudinally forward, y is to port, and z is vertically upward. The instantaneous velocity of the model is $U(t)$, where t is the time.

The water is assumed to be inviscid and incompressible with a velocity potential ϕ, which satisfies the Laplace equation:

$$\phi_{xx} + \phi_{yy} + \phi_{zz} = 0. \tag{2}$$

The linearized kinematic boundary condition on the free surface is

$$\phi_z - \zeta_t + U\zeta_x = 0 \quad \text{on} \quad z = 0. \tag{3}$$

The linearized Bernoulli equation on the free surface in the moving reference frame is

$$\phi_t - U\phi_x + g\zeta = 0 \quad \text{on} \quad z = 0, \tag{4}$$

where g is the acceleration due to gravity and ζ is free-surface elevation.

The combined free-surface condition is then

$$\phi_{tt} + U^2\phi_{xx} - 2U\phi_{xt} - \dot{U}\phi_x + g\phi_z = 0 \quad \text{on} \quad z = 0. \tag{5}$$

The kinematic condition on the sea bottom is

$$\phi_z = 0 \quad \text{on} \quad z = -d. \tag{6}$$

The tank-wall boundary condition is

$$\phi_y = 0 \quad \text{on} \quad y = \pm w/2, \tag{7}$$

in which w is the tank width.

The disturbance of the vessel is simulated by employing the usual thin-ship approximation for the centerplane source, namely,

$$\sigma = -U\frac{\partial b}{\partial x}, \tag{8}$$

where $b(x, z)$ is the local beam.

2.2. Unsteady resistance

The solution to the field equation and the relevant boundary conditions can be obtained through an application of a two-dimensional Fourier transformation from the x-y physical domain to the corresponding k_x-k_y wave-number domain. One also employs a Laplace transform in the time domain.

The analysis is similar to that presented by Doctors and Sharma (1972, 1973). The final result for the wave resistance, which is equivalent to that given by Lunde (1951, equation 16.18 or 18.10), but in the current notation, is:

$$R_W = R_{W,1} + R_{W,2} \tag{9}$$

$$R_{W,1} = \frac{\rho\dot{U}}{2\pi}\sum_{i=0}^{\infty}\epsilon\sum_{j=-\infty}^{\infty}\int_{S_0}\frac{\partial b}{\partial x}\,\mathrm{d}S\int_{S_0}\frac{\partial b'}{\partial x'}\,\mathrm{d}S'\,(-1)^j\left[\frac{1}{r} - \frac{1}{r'}\right] \tag{10}$$

$$R_{W,2} = \frac{2\rho g}{\pi w}\int_0^t U(\tau)\,\mathrm{d}\tau\int_0^{\infty}k_x^2\,\mathrm{d}k_x\sum_{i=0}^{\infty}\epsilon(u^2 + v^2) \times \cos[\omega(t-\tau)]\cos\{k_x[s(t) - s(\tau)]\}. \tag{11}$$

The first term in equation (9) relates to the inertia of the water and is simply proportional to its density ρ. This term equals the product of the acceleration and the thin-ship infinite-Froude-number added mass of the vessel. The integrals are effected over the centerplane area of the vessel S_0. The symbol $'$ is used to distinguish the source variables from the field variables. The two radial distances from the source point to the field point are

$$r = \sqrt{(x - x')^2 + (iw)^2 + (z - z' - 2jd)^2} \tag{12}$$

$$r' = \sqrt{(x - x')^2 + (iw)^2 + (z + z' + 2jd)^2}. \tag{13}$$

It can be demonstrated that as the Froude number approaches zero, the second term in equation (9) approaches twice the negative of the image-sink distribution. Thus, at such low speeds, one can model the hydrodynamics of the vessel using just a simpler, added-mass, concept.

The second term in equation (9) relates to wave effects. Here, $s(t)$ is the distance traveled from the start of the motion. We also have

$$\omega = \sqrt{gk\tanh(kd)}. \tag{14}$$

The wave numbers k_x and k_y are related to the circular wave number k and the wave angle θ through the relationship:

$$k_x + \mathrm{i}k_y = k\exp(\mathrm{i}\theta). \tag{15}$$

The summation factor ϵ and the transverse wave number k_y are given by the formulas:

$$\epsilon = \begin{cases} 1/2 & \text{for} \quad i = 0 \\ 1 & \text{for} \quad i \geq 1, \end{cases} \tag{16}$$

$$k_y = 2\pi i / w. \tag{17}$$

The index i of the summation in these equations has been dropped for the sake of simplicity.

Finally, the finite-depth wave functions in equation (9) are given by the formulas

$$u = \frac{P^+ + \exp(-2kd)P^-}{1 + \exp(-2kd)} \tag{18}$$

$$v = \frac{Q^+ + \exp(-2kd)Q^-}{1 + \exp(-2kd)}, \tag{19}$$

in which the Michell deep-water wave functions $P^{\pm}$ and $Q^{\pm}$ are

$$P^{\pm} + \mathrm{i}Q^{\pm} = \int_{S_0} b(x, z) \exp(\mathrm{i}k_x x \pm kz)\, \mathrm{d}S. \tag{20}$$

2.3. Steady resistance

For the case of steady motion, the result for the wave resistance from Doctors and Day (1995), is

$$R_W = \frac{2\rho g}{w} \sum_{i=0}^{\infty} \epsilon k_x^2 k (u^2 + v^2) \Big/ \frac{\mathrm{d}f}{\mathrm{d}k}, \tag{21}$$

where the dispersion relationship and its derivative are

$$f = k^2 - k k_0 \tanh(kd) - k_y^2 = 0 \tag{22}$$

$$\frac{\mathrm{d}f}{\mathrm{d}k} = 2k - k_0 \tanh(kd) - k k_0 d \operatorname{sech}^2(kd) \tag{23}$$

and the fundamental circular wave number is

$$k_0 = g/U^2. \tag{24}$$

2.4. Wehausen asymptotic resistance

For the sake of completeness, we present the final formula for the asymptotic unsteady component of the wave resistance from Wehausen (1964), in the current notation. This component is to be added to the steady resistance in equation (21):

$$\Delta R_W \simeq \frac{\sqrt{2}\rho g k_0 k_x^2}{8\pi} \cdot (u^2 + v^2) \times \frac{1}{A} \times [C^- \cos(A) + (1 - S^-) \sin(A)] \tag{25}$$

$$A = \frac{1}{4} k_0 [s(t) - s(t_0)]. \tag{26}$$

Here, the special functions are defined as

$$C^{\pm} \pm \mathrm{i}S^{\pm} = \frac{1}{4} k_0 \int_0^{t_0} U(\tau) \exp\left(\mathrm{i}\{\omega(t_0 - \tau) \pm k_x [s(t_0) - s(\tau)]\}\right) \mathrm{d}\tau. \tag{27}$$

In these formulas, t_0 is the time at the point the steady velocity is reached, after the completion of the acceleration phase of the motion. The various functions, such as u, v, $C^{\pm}$, $S^{\pm}$, and ω, are all evaluated for

$$k_x = \frac{1}{4} k_0 \tag{28}$$

$$k_y = 0. \tag{29}$$

2.5. Asymptotic studies

We devote this section to illustrate the importance of the physical dimensions of the towing tank on the expected unsteady effects on the wave resistance. The two parts of Fig. 2 are theoretical calculations for the case of a Wigley model that is accelerated at $\dot{U} = 0.1\ g$ up to a Froude number of 0.2. The specific resistance R_W/W is plotted as a function of the dimensionless time $t\sqrt{g/L}$, in which W is the weight of the model and L is its length.

Seven curves are plotted in Fig. 2 (top), for the case of deep water $d/L = \infty$. The first three curves (the three short-dashed lines with three different thicknesses) are quasi-steady predictions from equation (21) for three different dimensionless tank widths w/L. The notation QS is employed on the plot to indicate these three curves. These three curves are essentially identical, indicating the very little effect of tank width in this instance. Furthermore, the curves are constant in value after the steady speed is achieved, as required.

The fourth curve (the long-dashed line), indicated by the abbreviation *AS,* is the Wehausen asymptotic formula using equation (26) together with equation (21) (for a very wide tank $w/L = 20$).

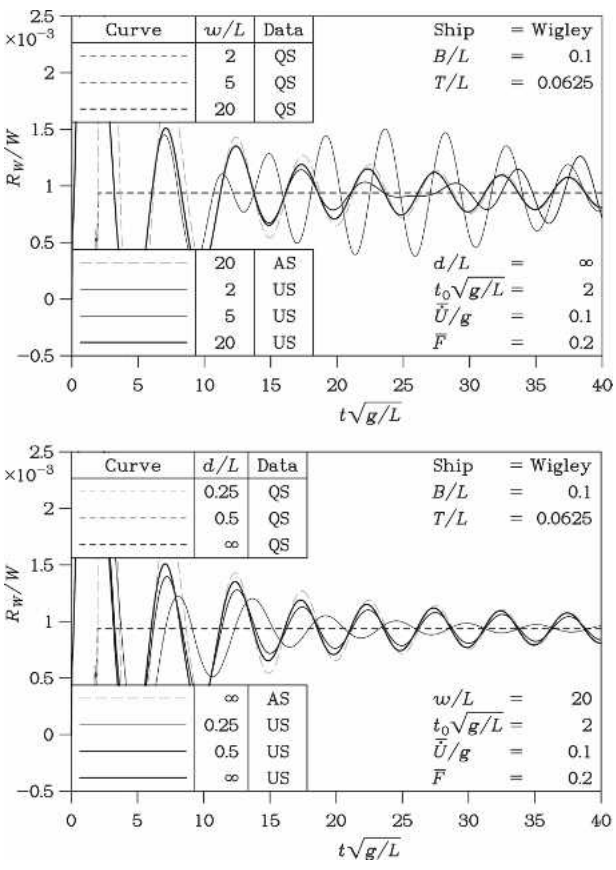

Fig. 2 Asymptotic studies. (Top) Influence of towing-tank width. (Bottom) Influence of water depth

The last three curves (continuous lines with three different thicknesses) were obtained from the true unsteady calculation in equation (9) and correspond to the three different tank widths noted earlier. One can observe that there is a very strong influence of tank width for these unsteady calculations, which is totally absent from the quasi-steady calculations. It is only for the last curve (when $w/l = 20$) that one can argue that the tank walls play a negligible role and nearly perfect agreement with the Wehausen results is achieved.

Figure 2 (bottom) is a summary of a study similar to that presented in Fig. 2 (top), except that a large tank width $w/L = 20$ is used and the effect of water depth is considered. It is seen that increasing the water depth has the effect of increasing the magnitude of the oscillations. When the dimensionless water depth d/L is greater than about 0.5, the condition is close to that of deep water. As for Fig. 4 (top), we may also note that, whereas the unsteady effects depend very strongly on the water depth, this is not true at all for the quasi-steady (steady) calculations.

3. Experiments

3.1. Experiment equipment

The experiment tests were carried out in the towing tank in the Acre Road Hydrodynamics Laboratory of the Universities of Glasgow and Strathclyde. The tank is 75.8 m long and 4.572 m wide; for the present tests, the depth was 2.330 m. The carriage drive was replaced in 2005; in the context of the present study, a key feature of the new digital control system for the carriage drive is the ability to set the target speed of the carriage using an analog input. Thus, the velocity history for a given run is generated in advance and then output into the carriage control system via a digital-to-analog converter. The actual speed of the carriage is measured from encoders on the motor drive shafts. Both signals were recorded. In order to take full advantage of this facility, the carriage drive had to be retuned; in order to achieve an appropriately rapid dynamic response, it was found that the control system had to be made considerably more responsive than would normally be thought desirable for steady speed tests. In other respects, the experiment setup was conventional and conformed to International Towing Tank Conference (ITTC) recommendations.

A full analysis of the uncertainty of the unsteady results was not carried out in the current study. However, an estimate based on the procedure typically utilized for a steady-resistance analysis (see Appendix) indicates that total uncertainty for the nondimensionalized resistance is likely to be less than 0.5%, while previous studies have shown that uncertainty of speed measurements is of the order of 0.1%.

The model was towed from a point on the stationary waterline at amidships using a towing post that can only generate horizontal forces and offers no restraint in vertical, trim, or heel displacements. The model was aligned in the centerplane of the tank using a conventional yaw guide. Towing force was measured using a conventional load cell. The sinkage and trim were measured using two linear variable differential transducers (LVDTs), one located at the towing point and the other located a known distance away. Five channels of data were thus recorded in total. Following normal practice at this facility, data were recorded for the entire run, from a period before the carriage started, through the acceleration phase, the constant-velocity phase, and the deceleration phase until the carriage stopped.

Because of the need to allow space for deceleration, it was decided to choose a towing distance (for the acceleration phase plus the constant-speed phase) of 48.0 m, or 16 model lengths, for the analysis of the experiments.

A total of four series of tests was conducted. In each series, a different form of the acceleration phase of the motion was selected. These are described in the following section. In all cases, the carriage was programmed to reach its steady-state speed according to simple algebraic functions, as described in equation (1).

3.2. Sample experiment runs

We turn now to Fig. 3, which shows the velocity-history curves for two runs. Figure 3 (top) depicts a run for which the nominal acceleration phase of the run consists of a constant acceleration of $\dot{U} = 0.08\ g$ until a Froude number of 0.3 is reached. The short-dashed line refers to the input signal to the carriage-drive system, while the continuous line represents the measured (output) motion of the carriage.

The analysis procedure includes the following two features: first, the velocity curves are numerically smoothed in order to remove the high-speed oscillations resulting from the mechanical vibrations in the system. Second, a simple horizontal (temporal) shift has been applied to match the input and output velocity-

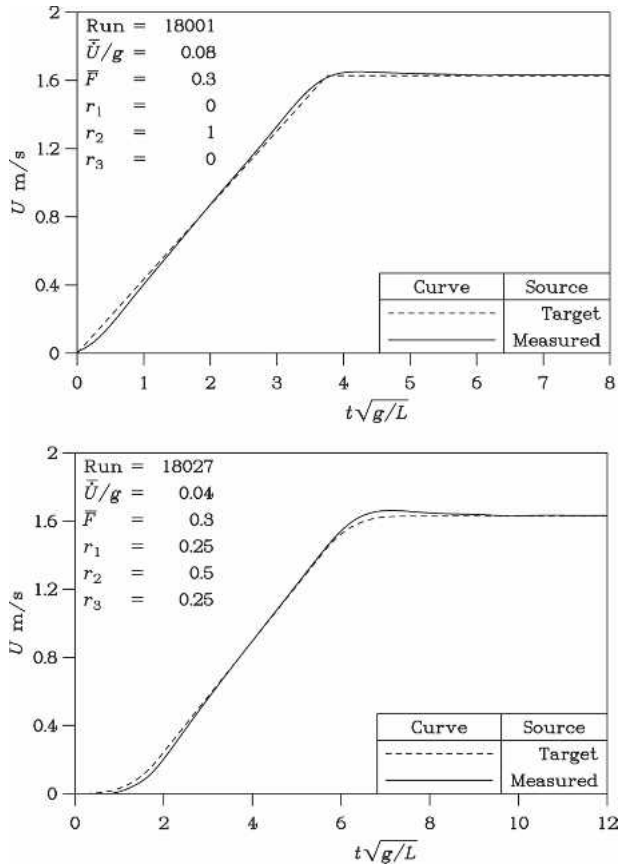

Fig. 3 Sample velocity histories. (Top) Constant acceleration. (Bottom) Double-sided smoothing

history curves when half the final velocity is reached. The carriage-control system is seen to suffer a small lag at the start of the run (when the input acceleration increases abruptly from zero in this challenging test case). Similarly, there is a small overshoot at the end of the acceleration phase.

For the purpose of plotting the metric results later in this paper, the nominal (input) acceleration, nominal steady velocity, and so on, were employed. On the other hand, the actual (smoothed) carriage velocity was used in the numerical calculations. Thus, a valid comparison between theory and experiment is ensured.

Figure 3 (bottom) shows a case less demanding of the carriage-control system. This example is one in which there is 25% smoothing ($r_1 = 0.25$) at the beginning of the acceleration phase and 25% smoothing ($r_3 = 0.25$) at the end of the acceleration phase. There is a better correlation between the input and output velocity histories here.

Two sets of results for the history of the specific resistance R_W/W as a function of the dimensionless distance traveled s/L are presented in Fig. 4. Figure 4 (top) shows the results for the case corresponding to the velocity history in Fig. 3 (top). A total of five curves is plotted.

The first two curves (indicated by the code "Expt" and plotted with the shortest-dashed lines) are derived from the experiments. The very first curve marked "Expt" is obtained implicitly from the formula:

$$R_T = R_W + R_H + R_F + R_A + R_I. \tag{30}$$

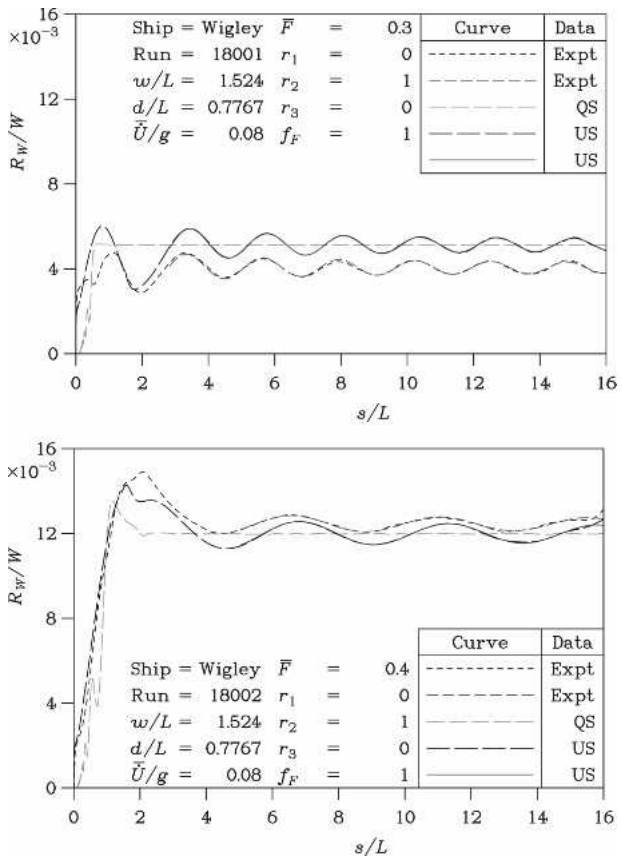

Fig. 4 Temporal wave-resistance curves. (Top) Froude number of 0.3. (Bottom) Froude number of 0.4

Here, R_T is the experiment total resistance, R_H is the transom resistance (zero in the case of a Wigley hull), R_F is the frictional resistance calculated by the 1957 ITTC formula, described by Lewis (1988, Section 3.5), and R_A is a correlation or roughness resistance (considered to be zero for the hydraulically smooth model used). Finally, R_I is the inertia (Newton) resistance of the vessel, being the product of the vessel mass and its instantaneous acceleration. This last term is also zero for the current investigation, because the analyses and comparisons of the experiment data were restricted to the steady-speed part of the runs.

It should be noted that, in the current study, the form factor was taken as unity. This may lead to a discrepancy in the mean total resistance; however, our interest here was focused on the oscillatory component of the wave resistance and, as such, is not of great importance.

The second curve marked "Expt" is the result of a Wehausen-type regression analysis, in which the following mathematical curve has been fitted using a nonlinear least-square-error procedure.

$$R_W(t) = R_{W,\infty} + \hat{R}_{W,0} \times \cos[(\omega(t - t_0) + \epsilon][\omega_\infty(t - t_0)]^N. \tag{31}$$

Here, $R_{W,\infty}$ corresponds to the quasi-steady resistance from equation (21), which is plotted as the third curve for reference purposes. Next, $\hat{R}_{W,0}$ is the nominal amplitude coefficient for the oscillations, ω is the radian frequency of the oscillation in the resistance curve, ϵ is the phase angle relative to the start of the steady-state part of the run in the towing tank, N is the decay factor, and ω_∞ is the Wehausen radian frequency of the oscillations obtained from equations (14), (28), and (29). That is:

$$\omega_\infty = g/2U. \tag{32}$$

For the purpose of this analysis, it was decided to fit the metric decay curve in equation (31) to the theoretical and experiment wave-resistance data, for points after one full Wehausen cycle after the start of the steady-velocity phase of the motion. This was a concession to the understanding that, in principle, the metric is to be applied for larger values of the time.

It can be observed that the second curve (the Wehausen-type decay curve) fits the experiment wave resistance very well over the range of data chosen for the analysis. This confirms that, in the current case at least, the commonly adopted practice of averaging the unsteady resistance to calculate the steady resistance is appropriate even in finite width and depth, and a short time after acceleration.

The third curve, denoted as QS, is the quasi-steady resistance as explained above.

The fourth curve, denoted by US, is the theoretical unsteady wave resistance computed from equation (9). The fifth and last curve, also denoted by US, is a Wehausen-type fit to the theory, using equation (31). This fifth curve is a good fit to the theoretical wave resistance.

It can be observed that in this case there is a vertical shift between the theoretical and experiment results. This is not unexpected, because it is well known that linear wave-resistance theory does not provide a perfect prediction of the experiment wave resistance. Additionally, the form resistance may contribute to this discrepancy. The simple additive decomposition implied by equation (30) is not exact either. Nevertheless, it is noteworthy that the

magnitude, frequency, and phasing of the oscillations appear to match well.

Finally, Fig. 4 (bottom) presents the equivalent results, but for a higher Froude number of 0.4. Similar comments about the excellent matching of the nature of the oscillations, between theory and experiment, can be stated in this case.

4. Results for the metrics

4.1. Influence of Froude number on metrics

In the first set of tests, the acceleration of the carriage was set at a constant value of 0.08 g during the acceleration phase. Different acceleration times were chosen in order to change the achieved steady-state Froude number, up to values of 0.5, and to study its effect on the nature of the expected oscillations in the wave-resistance curve.

Figure 5 (top left) shows the specific nominal amplitude of the oscillations as a function of the Froude number. The experiment points are indicated with symbols, and the theoretical calculation, using the full unsteady approach in equation (9), is indicated through a continuous line. The computed points are equal in number to the experiment points and are joined by straight lines.

According to the theory, the peak nominal amplitude of the oscillations occurs for $\overline{F} = 0.3$. Its value is very closely confirmed by the experiment. Note, also, that this particular experiment case was repeated. It can be observed that the repeatability of the experiment is high. In general, the trend of the theory matches that of the experiment. It is thought that the generally lower correlation between theory and experiment at the higher Froude numbers is due to the fact that there are few oscillations in the resistance over the length of the run. Thus, the matter of fitting a Wehausen-type decay curve in equation (31) becomes more problematic.

The decay coefficient is plotted in Fig. 5 (top right). The overall trend of the theory matches that of the experiments, although there is some scatter, which is proportionately greater at the higher Froude numbers. It is interesting to note that the decay coefficient N differs considerably from the Wehausen value of –1. The latter applies only to the case of an infinitely wide and deep tank.

Unfortunately, from the point of view of an experimental ship hydrodynamicist, it appears that the decay of the oscillatory variation in resistance is more gradual in the realistic case of finite tank dimensions and short time than in the idealized case analyzed by Wehausen. In some cases, it can be seen that the decay is extremely weak and, at the lowest speed, almost negligible.

The radian frequency of the oscillations is plotted in dimensionless form in Fig. 5 (bottom left). The nondimensionalizing frequency ω_∞ is the Wehausen value so that this presentation emphasizes differences from the case of unrestricted water. Overall, the agreement between theory and experiment is excellent, with a slight deterioration at the higher Froude numbers, as al-

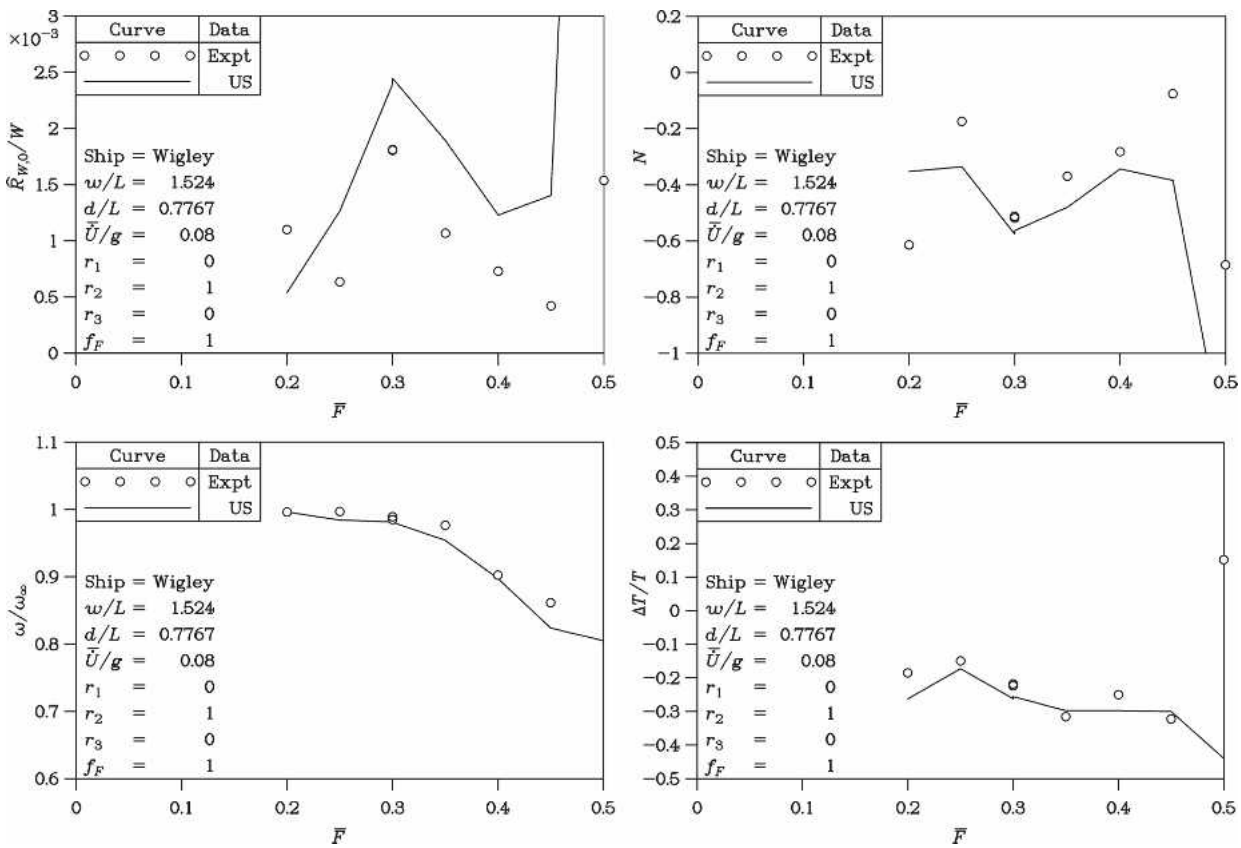

Fig. 5 Influence of Froude number on metrics. (Top left) Nominal amplitude. (Top right) Decay coefficient. (Bottom left) Radian frequency. (Bottom right) Phasing

ready noted. It can be seen that the greatest difference from the (simpler) Wehausen result is of the order of 20%.

Finally, the phasing of the oscillations is shown in Fig. 5 (bottom right). The phase ε in equation (31) is represented as a fraction of a cycle $\Delta T/T$ (between –1/2 and 1/2), relative to the start of the analysis of the metrics (at the point in time when the steady-velocity part of the motion commences).

4.2. Influence of acceleration on metrics

In the second set of tests, the steady-state Froude number was fixed at 0.3. Different rates of constant acceleration, between values of 0.01 g and 0.08 g, were selected for the first phase of the motion.

Figure 6 (top left) shows the amplitude of the oscillation. The agreement between theory and experiment is much better than that suggested in Fig. 5 (top left). Presumably, this is due to the restriction of this series of tests to a lower Froude number, for which the metric analysis is more reliable. Not surprisingly, one sees that a lower carriage acceleration leads to smaller oscillation amplitudes.

The decay factor is shown in Fig. 6 (top right). There is excellent agreement between theory and experiment for the higher levels of acceleration. For the lower levels of acceleration, there exists the difficulty in the metric analysis already noted; the available length of tank run for the metric analysis is less.

Figure 6 (bottom left) shows the frequency of the oscillation. The relative agreement between theory and experiment is excellent for all levels of acceleration considered.

Finally, Fig. 6 (bottom right) presents the phasing of the oscillations. Again, there is excellent agreement between theory and experiment for all levels of acceleration considered.

4.3. Influence of right-hand-side smoothing only on metrics

In the third set of tests, the steady-state Froude number was again fixed at 0.3. In these tests, the total time for the acceleration phase was fixed, giving a mean acceleration of 0.04 g. However, the first part of the acceleration phase was chosen to be zero in length ($r_1 = 0$), the second part of the acceleration phase involved a constant acceleration over a fraction $0 \leq r_2 \leq 1$ of the acceleration phase, and the third part of the acceleration phase r_3 involved a smoothing or blending, as described above in equation (1).

Figure 7 (top left) shows the amplitude of the oscillation. The overall agreement is good. The theory and the experiment both demonstrate that it is advantageous to shorten the second subphase of the acceleration and to use as much smoothing as possible for the third subphase.

The decay factor is plotted in Fig. 7 (top right). The agreement between theory and experiment is very good for the lesser amounts of acceleration smoothing (right-hand side of the graph).

Figure 7 (bottom left) shows the frequency of the oscillation. The agreement of theory and experiment is good over the range of the tests.

For this series of tests, there is a strong influence of smoothing on the phasing, as demonstrated by both the theory and the ex-

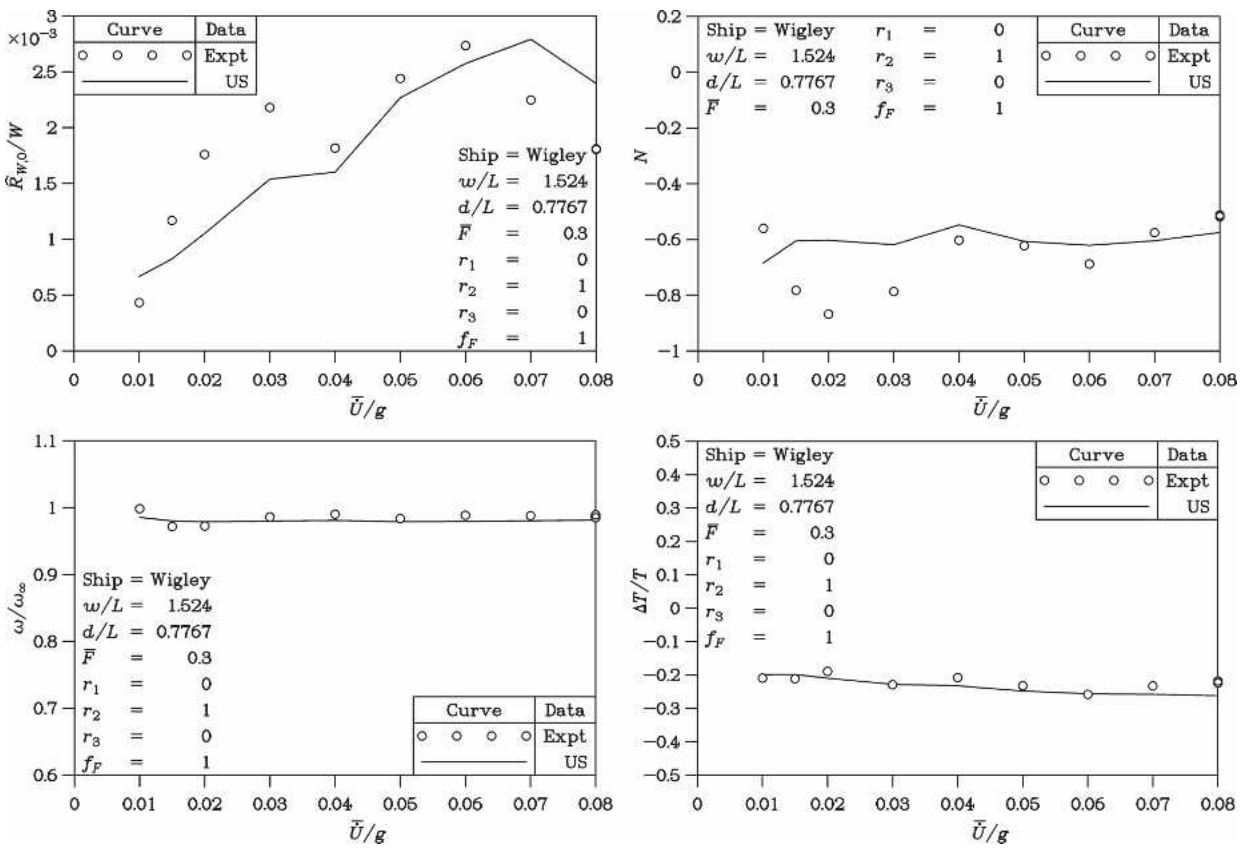

Fig. 6 Influence of acceleration on metrics. (Top left) Nominal amplitude. (Top right) Decay coefficient. (Bottom left) Radian frequency. (Bottom right) Phasing

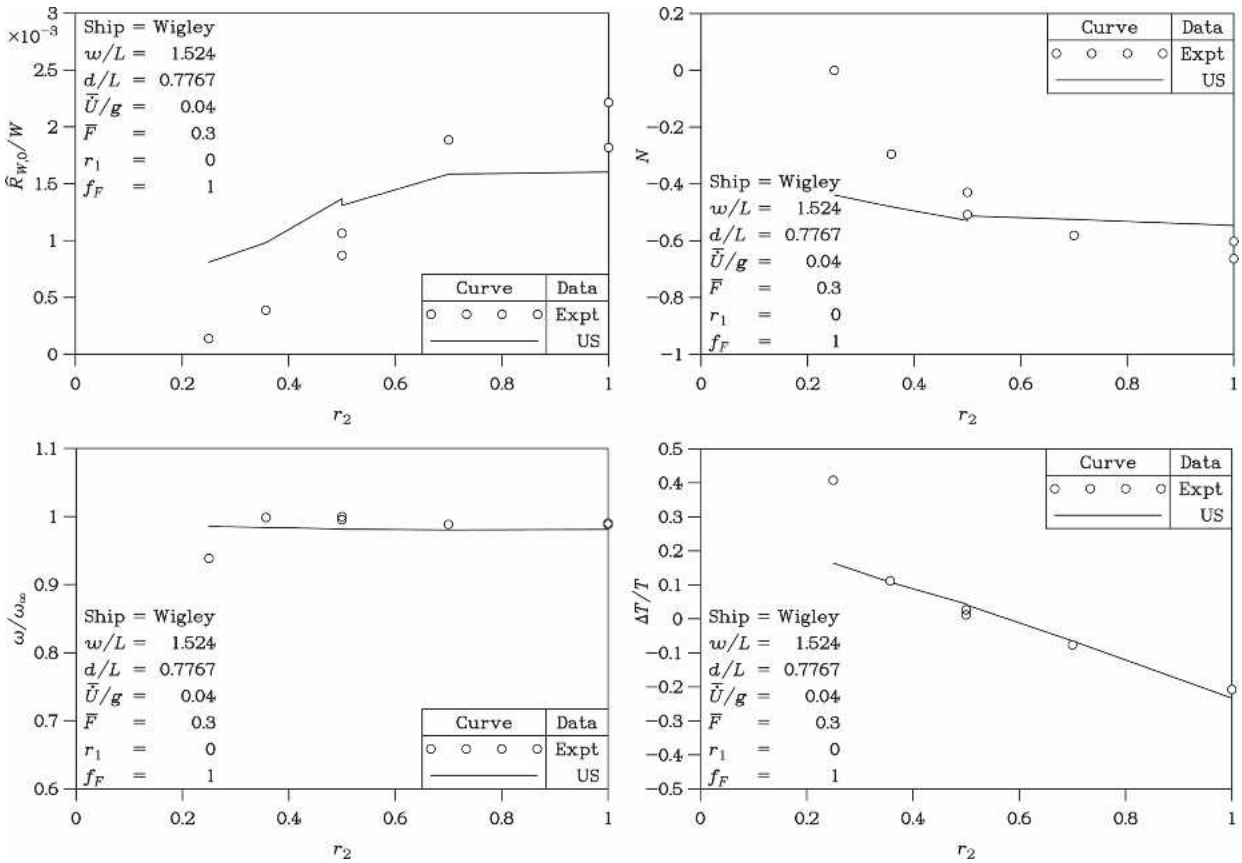

Fig. 7 Influence of right-hand-side smoothing on metrics. (Top left) Nominal amplitude. (Top right) Decay coefficient. (Bottom left) Radian frequency. (Bottom right) Phasing

periment in Fig. 7 (bottom right). The correlation is particularly high on the right-hand side of the graph.

4.4. Influence of two-sided smoothing on metrics

In the fourth and last set of tests, the steady-state Froude number was yet again fixed at 0.3. In these tests, the total time for the acceleration phase was also fixed, giving a mean acceleration of 0.04 g, as in the third set of tests. In this case, the acceleration phase was subdivided into three subphases: a smoothed part r_1, a constant-acceleration part of fixed duration $r_2 = 1/2$, and another smoothed part r_3. The proportion of the smoothed first subphase was varied from 0 to 1/2.

Figure 8 (top left) shows the amplitude of oscillation. Although the theory appears to be a little low in value over the central portion of the plot, it can be seen that decreasing the duration of the first subphase (the left-hand side of the plot) is advantageous for reducing the amplitude of the oscillations.

There is excellent agreement between theory and experiment in Fig. 8 (top right) for the decay coefficient, which varies little with the proportion of the subphases.

There is also good correlation between theory and experiment for the frequency of the oscillation in Fig. 8 (bottom left). In this example, the frequency is almost identical to the Wehausen value.

Figure 8 (bottom right) demonstrates remarkably good agreement between theory and experiment for the phasing of the oscillations, which is strongly affected by the proportion of the subphases of the acceleration.

5. Conclusions

5.1. Current work

This research has demonstrated that the unsteady thin-ship theory, which is an extension of the Michell (1898) theory to the case of unsteady motion, can provide relatively accurate predictions for the unsteady component of the wave resistance.

In general, both experiment and theoretical results have shown that the oscillation in the resistance time-history in a realistic towing tank test can be modeled by a formula of the general type suggested by Wehausen. However, the influence of tank width and tank depth, as well as the short time allowed in practice after acceleration has finished, changes the values of the coefficients in the equation. In the examples calculated, the rate of decay of the oscillations was considerably less than that suggested by the Wehausen formula; in some cases, the oscillations barely decay at all. Nonetheless, the results suggest that a good estimate of the steady wave resistance can be obtained from averaging the unsteady values over a whole number of cycles.

In some situations, there is perhaps less than satisfactory agreement between theory and experiment, such as for high Froude

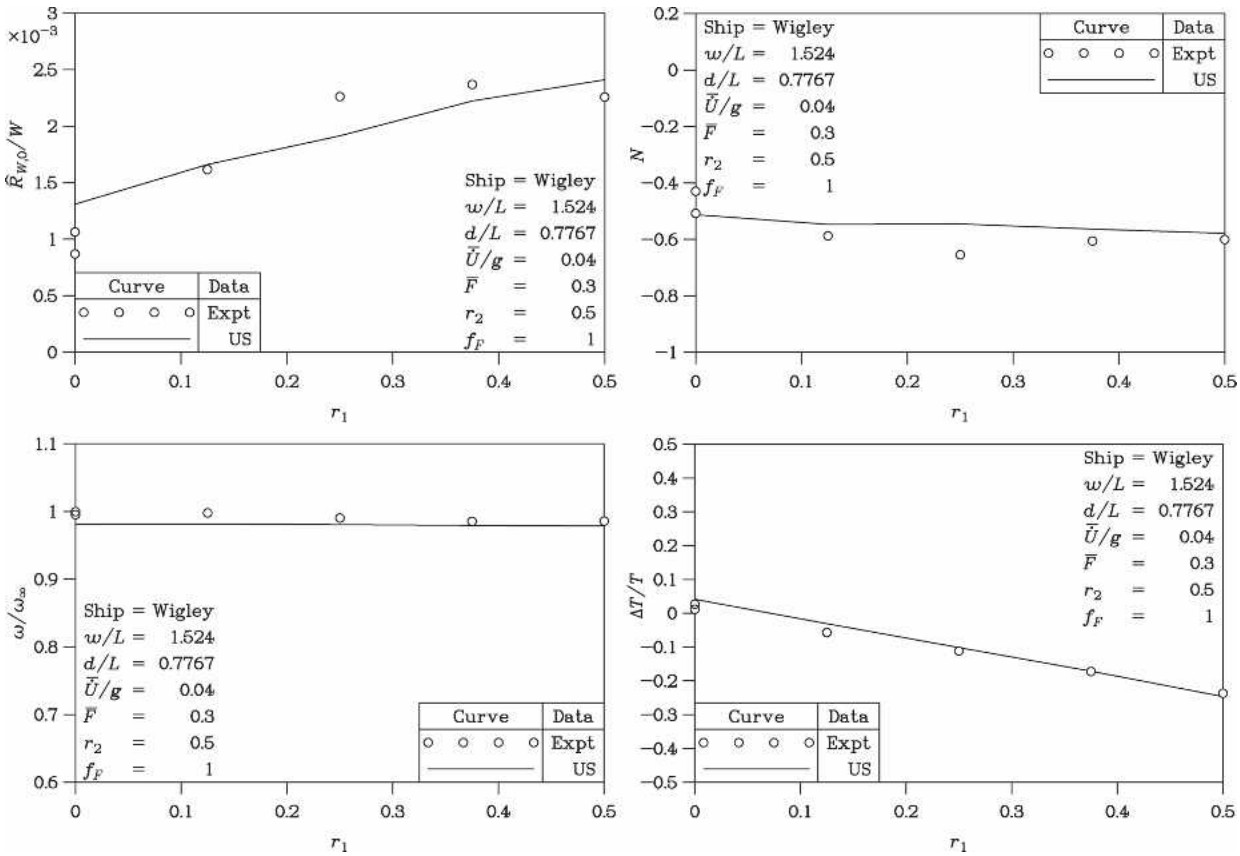

Fig. 8 Influence of two-sided smoothing on metrics. (Top left) Nominal amplitude. (Top right) Decay coefficient. (Bottom left) Radian frequency. (Bottom right) Phasing

numbers in Fig. 5 (top left, top right). In such cases, it is believed that the cause of the difficulty lies in the towing tank possessing insufficient length, creating difficulties with respect to an accurate fit of the Wehausen-type decay curve. That is, the coefficients in the decay might be very sensitive to the resistance data when there are only one or two cycles of the oscillation to process.

Despite this, it is encouraging to observe the excellent agreement for the other two parameters, namely, the frequency of the oscillations and their phasing.

5.2. Future work

This research has demonstrated that the characteristics of the oscillations in the wave resistance during a towing-tank test can be predicted with confidence. In particular, the magnitude and rate of decay of the oscillations are of interest to naval architects, who would, generally speaking, wish to minimize their effect.

A useful line of future work would be to determine velocity histories that would minimize the oscillations, given the available length of the tank.

The water depth used for this work was relatively great. It is known that particularly unusual effects occur when the steady-state depth Froude number is in the vicinity of unity. It would be an interesting second extension to this work to conduct such tests, because the unsteady theory can be applied equally well to this case.

Acknowledgments

We would like to thank The Universities of Glasgow and Strathclyde for providing the Sir David Anderson Bequest Award, which supported travel costs associated with this project. We would also like to express our appreciation to Mr. Charles Keay, Laboratory Coordinator, who supervised the construction of the ship model and the running of the towing-tank tests.

In addition, we also gratefully acknowledge the infrastructure support provided by The University of New South Wales.

References

ÇALIŞAL, S. 1977 Effect of initial acceleration on ship wave pattern and wake survey methods, JOURNAL OF SHIP RESEARCH, **21**, 4, 239–247.

DJACHENKO, V. K. 1970 *The Wave Resistance of a Surface Pressure Distribution in Unsteady Motion*, University of Michigan, Department of Naval Architecture and Marine Engineering, Report 44, January.

DOCTORS, L. J. 1972 The forces on an air-cushion vehicle executing an unsteady motion, *Proceedings,* 9th Symposium on Naval Hydrodynamics, August, Paris, France, vol. 1, 35–94, Discussion: 95–97.

DOCTORS, L. J. 1975 The experimental wave resistance of an accelerating two-dimensional pressure distribution, *Journal of Fluid Mechanics,* **72**, 3, 513–527.

DOCTORS, L. J. 1993 On the use of pressure distributions to model the hydrodynamics of air-cushion vehicles and surface-effect ships, *Naval Engineers Journal,* **105**, 2, 69–89.

DOCTORS, L. J., AND DAY, A. H. 1995 Hydrodynamically optimal hull forms for river ferries, *Proceedings,* International Symposium on High-Speed Vessels for Transport and Defence, Royal Institution of Naval Architects, November, London, England, 5.1–5.15.

DOCTORS, L. J., AND SHARMA, S. D., 1972 The wave resistance of an air-cushion vehicle in steady and accelerated motion, JOURNAL OF SHIP RESEARCH, **16**, 4, 248–260.

DOCTORS, L. J., AND SHARMA, S. D. 1973 The acceleration of an air cushion vehicle under the action of a propulsor, JOURNAL OF SHIP RESEARCH, **17**, 2, 121–128.

HAUSSLING, H. J., AND VAN ESELTINE, R. T. 1975 *Unsteady Air-Cushion Vehicle Hydrodynamics Using Fourier Series,* Naval Ship Research and Development Center, Computation and Mathematics Department, Report CMD-22-75, July.

HAUSSLING, H. J., AND VAN ESELTINE, R. T. 1978 Waves and wave resistance for air-cushion vehicles with time-dependent cushion pressures, JOURNAL OF SHIP RESEARCH, **22**, 3, 170–177.

ITTC. 2002 *Testing and Extrapolation Methods Resistance: Uncertainty Analysis Example for Resistance Test,* ITTC: Recommended Procedures and Guidelines: 7.5-02-02-02.

KARA, F., AND VASSALOS, D. 2005 Time domain computation of the wave-making resistance of ships, JOURNAL OF SHIP RESEARCH, **49**, 2, 144–158.

LEWIS, E. V., 1988 *Resistance, Propulsion and Vibration*, Principles of Naval Architecture, vol. 2, Society of Naval Architects and Marine Engineers, Jersey City, NJ.

LUNDE, J. K. 1951 On the linearized theory of wave resistance for displacement ships in steady and accelerated motion, *Transactions of the Society of Naval Architects and Marine Engineers,* **59**, 25–76, Discussion: 76–85.

LUNDE, J. K. 1953 *A Note on the Linearized Theory of Wave Resistance for Accelerated Motion,* Norges Tekniske Høgskole, Skipsmodelltanken, Report 27, September.

MICHELL, J. H. 1898 The wave resistance of a ship, *Philosophical Magazine,* London, Series 5, **45**, 106–123.

NAKOS, D. E., AND SCLAVOUNOS, P. D. 1990 On steady and unsteady ship wave patterns, *Journal of Fluid Mechanics,* **215**, 263–288.

SHEBALOV, A. N. 1970 *Theory of Ship Wave Resistance for Unsteady Motion in Still Water,* University of Michigan, Department of Naval Architecture and Marine Engineering, Report 67, March.

SIBUL, O. J., WEBSTER, W. C., AND WEHAUSEN, J. V. 1979 A phenomenon observed in transient testing, *Schiffstechnik,* **26**, 4, 179–200.

SRETENSKY, L. N. 1936 On the wave-making resistance of a ship moving along in a canal, *Philosophical Magazine,* Series 7, Supplement, **22**, 150, 1005–1013.

WEHAUSEN, J. V. 1964 Effect of the initial acceleration upon the wave resistance of ship models, JOURNAL OF SHIP RESEARCH, **7**, 3, 38–50.

WIGLEY, W. C. S. 1934 A comparison of experiment and calculated wave-profiles and wave-resistances for a form having parabolic waterlines, *Proceedings of the Royal Society of London,* Series A, **144**, 851, 144–159.

YEUNG, R. W. 1975 Surface waves due to a maneuvering air-cushion vehicle, JOURNAL OF SHIP RESEARCH, **19**, 4, 224–242.

Appendix: uncertainty of experiment results

In a "standard" towing test, the results for speed and resistance are averaged over a selected period during the steady-speed section of the run, and the result is typically presented in terms of a resistance coefficient. In such a case there are well-defined procedures that may be applied to estimate the uncertainty of the result (for example, ITTC, 2002). This uncertainty is generally considered to result from two components: bias, or systematic errors, and precision, or random errors.

In the current study, the time history of resistance during the run is considered rather than the mean value; as a consequence, the situation is somewhat different, particularly when the definition of the precision is considered. A full formal analysis of the precision would involve a substantial number of repeat runs, ideally with the model reinstalled several times, and would arguably require a point-by-point analysis of the variability of the data.

In the present case, then, the key components of uncertainty were examined using a technique developed for steady tests and used as a first estimate of the uncertainty in the unsteady tests; it is planned to carry out a formal uncertainty analysis in a future study. Since the results are presented in terms of resistance non-dimensionalized with respect to weight, the key uncertainties are those in resistance, model weight, and speed. In each case, both bias and precision should be considered.

The total bias in nondimensional resistance is given as:

$$(B_{R'})^2 = \left(\frac{\partial R'}{\partial R} B_R\right)^2 + \left(\frac{\partial R'}{\partial W} B_W\right)^2 = \left(\frac{1}{W} \cdot B_R\right)^2 + \left(-\frac{R}{W^2} \cdot B_W\right)^2 \tag{33}$$

where $R' = R/W$, and $B_{R'}$, B_R, B_W are the bias limits in nondimensional resistance, resistance, and weight, respectively.

The bias in resistance measurement B_R can be considered to stem from four major sources: the accuracy of the linear relationship fitted to the calibration data for the load cell, the accuracy of the weights used to calibrate the load cell, the accuracy of alignment of the load cell, and the error in the data-acquisition system.

Analysis of the calibration data, utilizing the procedure suggested in ITTC (2002), indicates that the standard error estimate (SEE) is better than 0.02 N, giving a confidence interval for the curve fit used to represent the performance of the load cell better than 0.04 N. The bias due to a single bit error in the A/D converter was of the order of 0.004 N. The load cell was calibrated with certified M1 weights, which have a minimum accuracy guaranteed to be better than 0.005%. The alignment of the load cell was measured to an accuracy of 0.1 deg, yielding a bias of 0.00015%. The load-cell alignment is independent of sinkage and trim. If a notional resistance value of 8.8 N is considered, giving $R/W \approx 12 \times 10^{-3}$, the total bias limit for resistance would be 0.0389 N.

Calibration data for the crane scales used to weigh the model, as supplied by the testing center responsible for the calibration, indicate a bias limit for the weight of the model of 0.105 N. The total bias limit in nondimensionalized resistance is thus calculated as:

$$(B_{R'})^2 = \left(\frac{1}{735.5} \cdot 0.0389\right)^2 + \left(-\frac{8.8}{735.5^2} \cdot 0.105\right)^2 = 5.3 \times 10^{-5}, \tag{34}$$

which is 0.44% of the notional value of $R/W \approx 12 \times 10^{-3}$. The largest contribution results from the bias in the load cell.

As discussed above, the precision was not explicitly addressed in the current study. However, in a related study, using identical equipment, with a different hull, the precision of the mean resistance was calculated using data from five repeat runs. Based on this data, the precision of resistance for a single run was estimated at 0.26%. In this case, the model was not reinstalled between runs; therefore, this figure does not include random errors due to ballasting, model alignment, trim, heel, or any other setup parameters.

Combining the bias and precision in the usual manner, the total uncertainty in nondimensionalized resistance at a notional resistance value of 8.8 N is thus estimated as 0.51% of the value.

Similar arguments can be applied to the speed. Calibration studies carried out at the facility, using a proximity sensor with targets accurately located using a machined length-bar, suggest that the bias is less than 0.1%. The same tests used to estimate precision for the resistance indicate a precision of mean speed for a single run of better than 0.05%, giving a total uncertainty of around 0.1%.

Although the calculation procedure described above clearly neglects some of the subtleties of the uncertainty in the unsteady tests, it is thought that the values presented give a plausible indication of the order of magnitude of the uncertainty of the measurements.